Symmetry, microscopy and spectroscopy signatures of altermagnetism

https://doi.org/10.1038/s41586-025-09883-2

Received: 28 February 2024

Accepted: 6 November 2025

Published online: 21 January 2026

Check for updates

Tomas Jungwirth[1,2]✉, Jairo Sinova[3], Rafael M. Fernandes[4,5], Qihang Liu[6], Hikaru Watanabe[7,8], Shuichi Murakami[9,10,11], Satoru Nakatsuji[7,12,13,14] & Libor Šmejkal[1,8,15]✉

The recent discovery of altermagnetism was in part motivated by the research of compensated magnets towards highly scalable spintronic technologies. Simultaneously, altermagnetism shares the anisotropic higher-partial-wave nature of ordering with unconventional superfluid phases, which have been at the forefront of research for the past several decades. These examples illustrate the interest in altermagnetism from a broad range of science and technology perspectives. Here we review the symmetry, microscopy and spectroscopy signatures of altermagnetism. We describe the spontaneously broken and retained symmetries that delineate altermagnetism as a distinct phase of matter with *d*-, *g*- or *i*-wave compensated collinear spin ordering. In materials ranging from weakly interacting metals to strongly correlated insulators, the microscopic crystal-structure realizations of the altermagnetic symmetries feature a characteristic ferroic order of anisotropic higher-partial-wave components of atomic-scale spin densities. These symmetry and microscopy signatures of altermagnetism are directly reflected in spin-dependent electronic spectra and responses. We review salient band-structure features originating from the altermagnetic ordering, and from its interplay with spin–orbit coupling and topological phenomena. Throughout, we compare altermagnetism with traditional ferromagnetism and Néel antiferromagnetism, and with magnetic phases with symmetry-protected compensated non-collinear spin orders. We accompany the theoretical discussions with references to relevant experiments.

Altermagnetism is a recently identified ordered phase of electrons and their spins in condensed matter[1,2]. The distinctive signatures of altermagnetism can be illustrated on simplified model structures, shown in Fig. 1. As a reference, ferromagnetism, carrying a finite net magnetization, is represented by a parallel (ferroic) alignment of atomic magnetic dipoles formed by electron spins in the position space of the crystal. The corresponding electronic spectrum in the momentum space is split into majority and minority channels with opposite spin. In contrast, altermagnetism with its compensated spin ordering is illustrated in Fig. 1 by a model highlighting the presence of an anisotropic component of the local spin density whose sign alternates on the atomic scale. The ferroic crystal order of these local anisotropic spin-density components has its counterpart in the alternating-sign spin polarization in the momentum space. The corresponding electronic spectrum has a form of equal-size, anisotropically distorted and mutually rotated energy isosurfaces of the opposite spin channels, intersecting at spin-degenerate nodes[1–3].

The microscopic mechanism of the spontaneous spin ordering in magnetic ground states, including altermagnetic, is due to an interplay of the spin-independent electron–electron Coulomb interaction in the many-body Hamiltonian with the Pauli exclusion principle. The mechanism is commonly referred to as the exchange interaction. Owing to a large energy scale of typical exchange interactions, the spin orders tend to be robust. In contrast, microscopic mechanisms by which the isotropic electron–electron Coulomb interaction can lead to ordered ground states with a spontaneously developed anisotropy have been considered to be of a more subtle correlated nature[4]. Here the prominent examples are the unconventional *d*-wave superconductivity in cuprates or the *p*-wave superfluidity of ^{3}He (Fig. 1c,d). Altermagnetism stands apart from these anisotropic ordered phases driven by the subtle correlated instabilities in metallic Fermi fluids[4]. The anisotropic spin ordering in altermagnets is commonly stabilized by a robust microscopic mechanism. It originates from a direct interplay of, on the one hand, the exchange interaction and, on the other hand,

[1]Institute of Physics, Czech Academy of Sciences, Prague, Czech Republic. [2]School of Physics and Astronomy, University of Nottingham, Nottingham, UK. [3]Institut für Physik, Johannes Gutenberg Universität Mainz, Mainz, Germany. [4]Department of Physics, The Grainger College of Engineering, University of Illinois Urbana-Champaign, Urbana, IL, USA. [5]Anthony J. Leggett Institute for Condensed Matter Theory, The Grainger College of Engineering, University of Illinois Urbana-Champaign, Urbana, IL, USA. [6]Department of Physics, State key laboratory of quantum functional materials and Guangdong Basic Research Center of Excellence for Quantum Science, Southern University of Science and Technology, Shenzhen, China. [7]Department of Physics, University of Tokyo, Tokyo, Japan. [8]Max Planck Institute for the Physics of Complex Systems, Dresden, Germany. [9]Department of Applied Physics, University of Tokyo, Tokyo, Japan. [10]International Institute for Sustainability with Knotted Chiral Meta Matter (WPI-SKCM2), Hiroshima University, Higashi-hiroshima, Japan. [11]Center for Emergent Matter Science, RIKEN, Saitama, Japan. [12]Institute for Solid State Physics, University of Tokyo, Kashiwa, Japan. [13]Institute for Quantum Matter and Department of Physics and Astronomy, Johns Hopkins University, Baltimore, MD, USA. [14]Trans-scale Quantum Science Institute, University of Tokyo, Tokyo, Japan. [15]Max Planck Institute for Chemical Physics of Solids, Dresden, Germany. ✉e-mail: jungw@fzu.cz; lsmejkal@pks.mpg.de

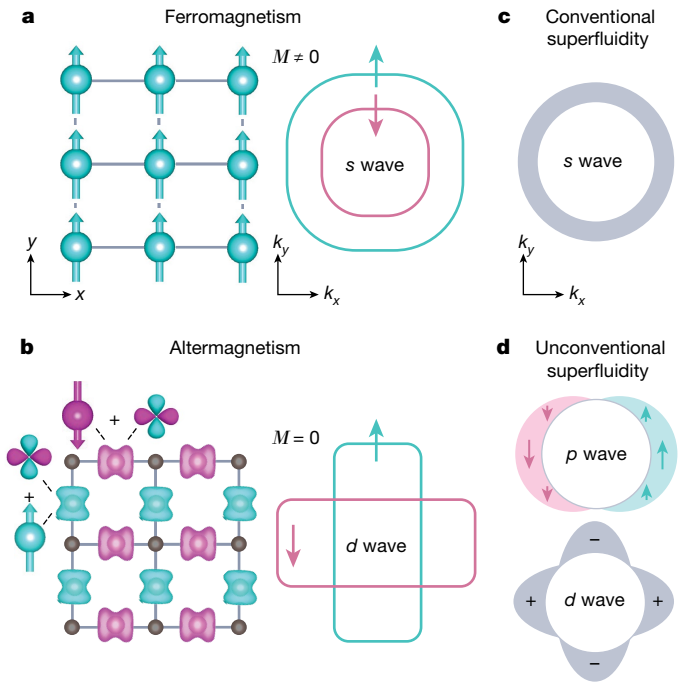

Fig. 1 | Ferromagnetism and altermagnetism versus conventional and unconventional superfluidity. a, Cartoon of uncompensated ($M \neq 0$) ferromagnetism with a parallel (ferroic) alignment of atomic magnetic dipoles in the position space of the crystal and corresponding majority-spin and minority-spin energy isosurfaces in the momentum space preserving the crystallographic point-group rotation symmetry (*s*-wave). *M* labels magnetization, and k_x and k_y are components of the electron momentum. **b**, Cartoon of compensated ($M = 0$) altermagnetism with depicted decomposition of the local anisotropic spin density[1–3] into a dipole (circle with arrow) and a higher-partial-wave (*d*-wave) spin-density component. Cyan and magenta colours mark opposite spin polarizations. The higher-partial-wave (*d* wave) component is ferroically ordered on the crystal. The depicted model is a 2D Lieb lattice[7,8,113,114]. The momentum-space spin-up and spin-down energy isosurfaces show the corresponding anisotropic (*d* wave) order breaking the *T* symmetry[1–3]. They intersect at spin-degenerate nodes. **c**, Cartoon of the isotropic scalar order parameter and the quasiparticle gap function (filled area) on the Fermi surface for conventional *s*-wave superfluidity (superconductivity). **d**, Top: anisotropic order parameter (arrows) and the quasiparticle gap (filled area) for unconventional *p*-wave superfluidity. The *p*-wave order parameter is a collinear vector in the spin space, reminiscent of collinear altermagnetism, but has odd parity. Bottom: anisotropic order parameter (±) and the quasiparticle gap (filled area) for unconventional *d*-wave superfluidity. The *d*-wave order parameter has even parity, reminiscent of altermagnetism, but is a scalar in the spin space (no spin order). For a detailed comparison between altermagnetism and unconventional superfluidity, see ref. 4.

the single-particle electron interaction with the ionic potential of the underlying crystal lattice with a suitable symmetry[1,2,4]. As a result, altermagnetism can form at ambient conditions and in a variety of metallic, as well as insulating, materials. This has opened a range of research directions exploring the extraordinary properties and responses enabled by altermagnetism, and the synergies of altermagnetism with other condensed-matter phases[1,2,5–30]. (For more details on the research context and additional references, see Supplementary information).

In the following sections, we review the distinctive symmetry, microscopy and spectroscopy signatures of the altermagnetic ordering that underpin the emerging broad research of this recently identified phase of matter. For other review, perspective or commentary articles focusing on altermagnetism in the context of the symmetries of compensated magnets, the anomalous Hall effect and other spintronic responses, the initial experimental research, or discussing distinctions between altermagnetism and correlated metallic and superfluid instabilities of Fermi liquids, we point to refs. 2,4,31–35.

Symmetry signatures

The single-particle interaction term of the electronic Hamiltonian owing to the ionic potential of the crystal lattice has no explicit dependence on the electron spin. It is, therefore, invariant under the symmetry group SO(3) of all continuous spin-space rotations. In the real space, the crystal potential obeys symmetries of the crystallographic group *G*. The many-body term in the Hamiltonian owing to the electron–electron interactions has also no explicit dependence on spin, that is, has the spin-space SO(3) symmetry, plus it is isotropic in the real space. The normal phase of the electronic system determined by these interaction terms retains the full symmetry, $Z_2^T \times \mathrm{SO}(3) \times G$, of the corresponding Hamiltonian. Here we also explicitly included the time-reversal (*T*) symmetry via the Z_2^T group containing *T* and the identity.

Conventional collinear ferromagnetism, represented by the model spin arrangement on the crystal in Fig. 1a, spontaneously breaks (some) spin-space SO(3) symmetries and the *T* symmetry. Simultaneously, the retained symmetries in the ordered ground state are given by the spin group $Z_2^{C_2T} \ltimes \mathrm{SO}(2) \times G$. Here the C_2T symmetry in $Z_2^{C_2T}$ combines *T* with a two-fold spin-space rotation C_2 around an axis orthogonal to the collinearity axis of spins, and SO(2) is a group of continuous spin-space rotations around the collinearity axis.

The altermagnetic ordering[1] (Fig. 1b) also spontaneously lowers the Hamiltonian's $Z_2^T \times \mathrm{SO}(3)$ symmetry to the $Z_2^{C_2T} \ltimes \mathrm{SO}(2)$ symmetry of the ground state. (This part of the spontaneous symmetry lowering is common to all collinear spin-ordered phases[1,36,37]). In contrast to ferromagnetism, however, the altermagnetic ordering retains only symmetries of a halving subgroup *H* of the crystallographic group *G*. The other half of the symmetries contained in $G - H$ are spontaneously broken on their own, whereas the altermagnetic ground state retains symmetries combining the crystallographic transformations from $G - H$ with the spin-space rotation C_2 around an axis orthogonal to the spins. In the case of the altermagnetic order, $G - H$ contains real-space rotation transformations (proper or improper and symmorphic or non-symmorphic) and does not contain the real-space inversion (parity *P*) or a translation (*t*). With this constraint, the altermagnetic-ordering class is unambiguously and exclusively delineated by the spin groups of the form[1], $Z_2^{C_2T} \ltimes \mathrm{SO}(2) \times ([E\|H] + [C_2\|G - H])$. (Here *E* is the spin-space identity and the spin-space and real-space symmetry transformations are on the left and right of the double bar in the square bracket, respectively).

The $[C_2\|G - H]$ symmetries imply that the altermagnetic spin ordering is compensated, that is, that the integrated spin-up and spin-down densities have the same magnitude. The $[E\|H]$ term implies that in each spin channel, the spin density is anisotropic. The altermagnetic spin ordering retains the symmetries of the halving subgroup *H*, while spontaneously breaking the remaining $G - H$ rotation symmetries.

Before we turn to the discussion in the following sections on how the altermagnetic spin-group symmetries are reflected in the position-space microscopy and momentum-space spectroscopy signatures, we conclude this section with a brief comment on the physical distinction between symmetry breaking by the spin ordering and the spin–orbit coupling.

The spin ordering can occur in ground states of many-body systems of interacting electrons by spontaneously breaking the spin-space SO(3) symmetry of the spin-independent crystal-potential and the electron–electron interaction terms in the Hamiltonian[1,38–41]. We note here that the corresponding spin-ordered ground state is degenerate as different ordered states related by any spin-rotation transformation from the SO(3) symmetry group of the Hamiltonain have the same energy.

Box 1

Comparison of spin groups and magnetic groups

In the figure, we compare the spin groups[1,36] of a collinear uncompensated spin ordering in Fe, a collinear compensated spin ordering in (altermagnetic) NiF_2, and a non-collinear coplanar compensated spin ordering in Mn_3Sn, with the magnetic groups[200] of the three structures. The spin group is a direct product of the so-called spin-only group and the so-called non-trivial spin group[1,36,37]. The spin-only group distinguishes the collinear (Fe and NiF_2) from the non-collinear coplanar (Mn_3Sn) spin orders, where in the former case the spin-only group is given by $Z_2^{C_2T} \ltimes \mathrm{SO}(2)$ and in the latter case by $Z_2^{C_2T}$. The non-trivial spin group for the uncompensated spin ordering (Fe) has no term combining a crystallographic transformation with a spin rotation. In contrast, such a combined transformation is present in the case of the compensated spin ordering (NiF_2, Mn_3Sn).

Unlike the spin groups, the magnetic groups for all three structures are the same. This illustrates, among other features, that the magnetic groups do not generally distinguish between the collinear and the non-collinear (coplanar or non-coplanar) magnets. In addition, the specific magnetic group of the three structures belongs to the so-called ferromagnetic groups, which allow for a net magnetization. All three structures are thus rendered as uncompensated by the magnetic group. A comparison with the respective spin groups shows that in the case of NiF_2 and Mn_3Sn, the net magnetization is of the relativistic spin–orbit-coupling origin, whereas the spin ordering alone yields a zero net magnetization in the non-relativistic limit protected by the spin-group symmetry. In the case of Fe, a non-zero net magnetization is allowed without the spin–orbit coupling by the spin-group symmetry. All three magnetic structures in the figure have spin-group symmetries that allow for spin-split electronic spectra in the absence of the spin–orbit coupling. In general, spin-group symmetries (and not magnetic-group symmetries) determine whether and at what momenta the non-relativistic band structure can be spin split, or whether spin-degeneracy of the non-relativistic bands is symmetry-enforced across the whole Brillouin zone.

Crystal structure	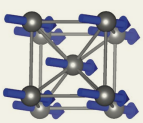 Fe ($M \parallel [110]$)	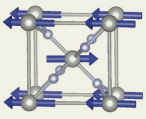 NiF_2	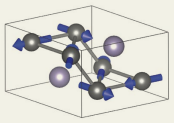 Mn_3Sn
Spin ordering	Collinear uncompensated	Collinear compensated	Coplanar compensated
Spin-only group	$\mathrm{SO}(2) \ltimes Z_2^{C_2T}$	$\mathrm{SO}(2) \ltimes Z_2^{C_2T}$	$Z_2^{C_2T}$
Non-trivial spin point group	${}^{1}m^{1}\bar{3}^{1}m$	${}^{2}4/{}^{2}m^{2}m^{1}m$	${}^{3z}6_3/{}^{1}m^{2x}m^{2xy}m$
Ferromagnetic point group	$m'm'm$	$m'm'm$	$m'm'm$

Box Fig. 1 | Spin groups and magnetic groups. Examples of collinear or non-collinear and compensated or uncompensated spin ordering with denoted corresponding spin-only group, non-trivial spin point group and magnetic point group. The middle column represents altermagnetism.

The spin–orbit coupling refers to single-particle interaction term(s) in the relativistic Hamiltonian that explicitly depend on the electron spin and that couple the spin-space and the real-space degrees of freedom[42]. In the case of the spin–orbit coupling, the spin-space SO(3) symmetry is thus already broken in the Hamiltonian of the electronic system. This makes the physical nature of the symmetry breaking by the spin–orbit coupling principally distinct from the spontaneous symmetry breaking by the spin ordering. Albeit typically weak compared with the crystal-potential and electron–electron interaction terms in materials without heavy elements, the spin–orbit coupling can have important consequences for equilibrium and non-equilibrium properties of the electronic systems. For example, in normal states of systems with broken P symmetry it can lift the spin degeneracy of the electronic spectra, or in magnets it can lift the degeneracy of the spin-ordered ground states[43,44]. It can also facilitate a range of topological band structure and transport phenomena[45–51].

The primary focus of this Review is on the physics associated with the altermagnetic spin ordering, but we also give examples of the interplay of the altermagnetic ordering with the spin–orbit coupling. On the symmetry level, the effects of the spin–orbit coupling are disentangled from the spin-ordering physics by employing the spin-group and the magnetic-group formalisms. In the spin-group formalism[1,2,36,37,52–69], focusing on the spin ordering alone, the symmetry transformations applied simultaneously in the spin space and in the real space can be different, reflecting the absence of any explicit spin dependence in the crystal-potential and the electron–electron interaction terms in the Hamiltonian. In contrast, the magnetic-group formalism[44,70] considers only a simultaneous application of the same symmetry transformations in both the spin space and the real space, reflecting the explicit coupling of the spin-space and the real-space degrees of freedom in the relativistic spin–orbit-coupled Hamiltonian. The complementary merits of the two symmetry formalisms are illustrated in Box 1.

Microscopy signatures

In this section, we look how the altermagnetic spin-group symmetries are realized on the microscopic level in representative crystal structures, and discuss the microscopic physics of ordering in altermagnets. Figure 2a shows the arrangement of anisotropic atomic spin densities in an altermagnetic rutile crystal obtained from microscopic theory[3]. These local spin densities can be decomposed into s-wave (dipole) components with antiparallel alignment between neighbouring atoms, and d-wave components aligned ferroicly on the crystal lattice, as schematically indicated in Fig. 2a. The d-wave spin-density components correspond to the d-wave symmetry of anisotropic exchange interactions in the rutile crystal lattice[56]. The ferroic order of the local d-wave spin-density components generates the T-symmetry-breaking electronic structure and responses, reminiscent of the effects of the ferroic order of local dipoles in conventional ferromagnets[3]. In contrast to the ferroicly ordered dipoles, however, the higher-partial-wave ferroic order does not generate a net magnetization and leads to the characteristic anisotropy of the phenomena observed in altermagnets.

We note that experimental signatures of the magnetic ordering in RuO_2, a metallic rutile crystal considered among this class of altermagnetic candidates from the early theoretical studies[3], are currently a matter of debate[71–88]. These seemingly controversial reports can be possibly explained by the magnetic order in ruthenates, including RuO_2, being fragile with respect to impurities, disorder or strain[82]. In other insulating rutile crystals[2,89–93], such as altermagnetic NiF_2 mentioned

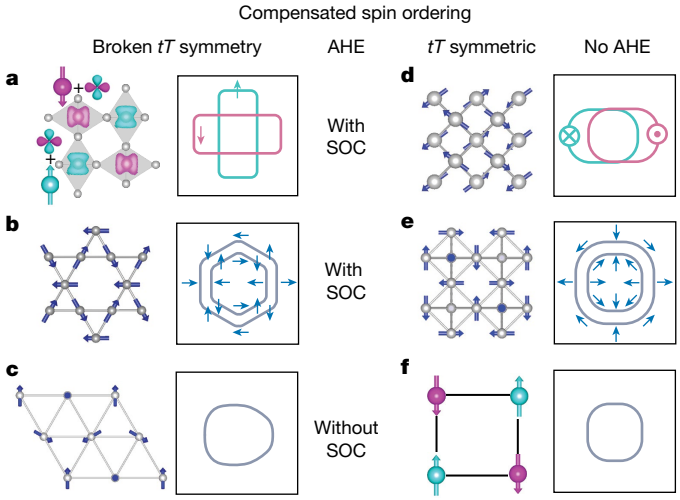

Fig. 2 | Magnets with compensated spin ordering. a, Left: altermagnetic ordering on a rutile crystal (RuO_2, FeF_2 and so on)[1–3] with anisotropic atomic spin densities schematically decomposed into antiparallel isotropic *s*-wave (dipole) and ferroically ordered anisotropic *d*-wave components. Right: corresponding *d*-wave order on the schematic momentum-space energy isosurfaces. **b**, Position-space (left) and momentum-space (right) cartoons of a non-collinear coplanar even-parity magnetic order represented by Mn_3Sn (refs. 148,158). **c**, Non-coplanar magnetic order in position space with a corresponding spin-degenerate electronic structure in the momentum space represented, for example, by CoM_3S_6 (M = Ta or Nb)[64,67,132,151,199]. **d**, Non-collinear coplanar magnetic order in the position space with corresponding odd-parity (*p* wave) collinear spin order in the momentum space represented by CeNiAsO (ref. 59). **e**, Non-collinear non-coplanar magnetic order in the position space with corresponding odd-parity non-collinear spin order in the momentum space represented by Ce_3InN (ref. 60). **f**, Conventional collinear Néel antiferromagnetism with the antiferroic order (*tT* symmetry) of opposite atomic dipole moments on an even number of crystal sublattices[117], and corresponding spin-degenerate electronic structure in the momentum space. Cartoons in all panels are for non-relativistic electronic structures. Whether or not the anomalous Hall effect is allowed (AHE or no AHE), and whether with or without the relativistic spin–orbit coupling (with or without SOC) is also indicated for all panels.

in Box 1, the experimental signatures of the compensated collinear magnetic order are well established.

An analogous decomposition of the local atomic spin densities applies to semiconducting and metallic room-temperature altermagnets MnTe and CrSb (ref. 94), which have become workhorse materials in theoretical and experimental research of altermagnetism[1,2,55,95–109]. In these crystals, the antiparallel alignment of local atomic dipoles is complemented by the ferroic order of local *g*-wave components of the anisotropic spin density[94], as schematically indicated in Fig. 3a. It is noted that the corresponding anisotropic exchange interactions were predicted[56] and experimentally demonstrated[110] in MnTe to generate alternating chiral splitting of the magnon spectra.

Recently, the family of experimentally confirmed altermagnets has been extended by KV_2Se_2O and RbV_2Te_2O layered crystals[111,112], shown in Fig. 3g. They feature atomic and spin arrangements corresponding to the two-dimensional (2D) Lieb-lattice model of *d*-wave altermagnetism[7,8,113,114], introduced in Fig. 1b. Lieb-lattice altermagnetism was also shown to be realized in the Mott insulating compound $La_2Mn_2Se_2O_3$ (ref. 115).

Remarkably, the altermagnetic symmetries can be realized by the ferroic order of the local *d*-wave (or higher even-parity-wave) spin densities on magnetic atoms without any local atomic dipole components[94]. Microscopic calculations identified such a pure form of atomic *d*-wave altermagnetism[94] in a Mott-insulator Ba_2CaOsO_6 (refs. 94,116). This underlines the microscopic distinction of altermagnetism from conventional Néel antiferromagnetism, where the latter has a characteristic antiferroic order (*tT* symmetry) of atomic dipole moments on an even number of crystal sublattices[117] (Fig. 2f).

Other microscopic mechanisms include the realization of the altermagnetic symmetries by crystal lattice deformations[7,118,119]. Although in the unperturbed crystal the opposite spin densities are related by one of the symmetries excluding the altermagnetic order (translation or inversion), the deformation, such as a twist of crystal planes, breaks these symmetries while obeying the altermagnetic spin-group symmetry.

There can also be cases where the role of symmetries of the single-particle potential of the ionic crystal lattice are complemented by electronic correlations in the formation of the altermagnetic phase. Here the altermagnetic phase is enabled by correlation-induced orbital ordering, which lowers the symmetry of the crystallographic group, compared with the symmetry of the ionic lattice. Together with the spin ordering by the exchange interaction, the phase then falls into the altermagnetic spin-group class[120,121].

Apart from this microscopic mechanism, the role of electronic correlations in promoting or affecting altermagnetism has been studied in various contexts[120,122–125], including the strongly coupled regime where the interaction strength is comparable to the bandwidth[126,127]. As the strongly correlated Mott-insulator crystals frequently display a compensated antiparallel magnetic order, several Mott insulating materials with appropriate spin symmetries have been put forward as altermagnetic candidates. Specifically, a wide class of Mott insulating perovskites, such as the manganite $CaMnO_3$ and the titanate $LaTiO_3$ (refs. 1–3,23,121,128), have been identified as platforms to realize and investigate altermagnetism in the regime of strong correlations. In these compounds, the oxygen octahedra rotate to accommodate the cation, lowering the ideal cubic symmetry of the perovskite down to orthorhombic, which essentially changes the spin group to altermagnetic. In different contexts, earlier studies found that the octahedra rotation in the perovskites can directly impact orbital degrees of freedom, which in turn affect the magnetic interactions[90,129]. Subsequent studies made the observation of the *T*-symmetry-breaking electronic structure and responses, and the identification of altermagnetism in these systems[1–3,23,121,128].

Similarly, Mott insulating states realized in oxides with other Ruddlesden–Popper phases, such as the cuprate La_2CuO_4 (ref. 1) and the nickelate $La_3Ni_2O_7$ (ref. 23), possess the spin-symmetry requirements to display altermagnetism. Besides three-dimensional (3D) oxides, 2D organic charge-transfer salts can also realize a Mott insulating altermagnetic phase owing to the fact that their organic molecules can form an arrangement similar to the Shastry–Sutherland lattice[127].

Spectroscopy signatures

An unconventional spin splitting that breaks the *T* symmetry in theoretical band structures of compensated magnets was initially reported in several coplanar[130], non-coplanar[131] and collinear[3] magnets. Employing the spin-group formalism[1,36,52–69,132] then enabled to disentangle by symmetry the spin-ordering and the spin–orbit coupling contributions to this unconventional spin splitting; the same applies to other previous theoretical reports of non-relativistic electronic structures with momentum-dependent spin splitting in compensated magnets[89–92,133,134].

Within the collinear magnets, the spin groups allowed the delineation of altermagnetism, as discussed in the previous sections. Numerous candidate materials with altermagnetic band structures have been identified based on the spin groups when analysing, for example, the published magnetic structures in the MAGNDATA database on the Bilbao Crystallographic Server[1,2,32,57,69,135]. Besides the numerous 3D inorganic crystals, the spin groups also enabled to establish the altermagnetic symmetry in the spectra of earlier studied or recently identified 2D[2,7,8,54,136–140] or organic[127,134] materials.

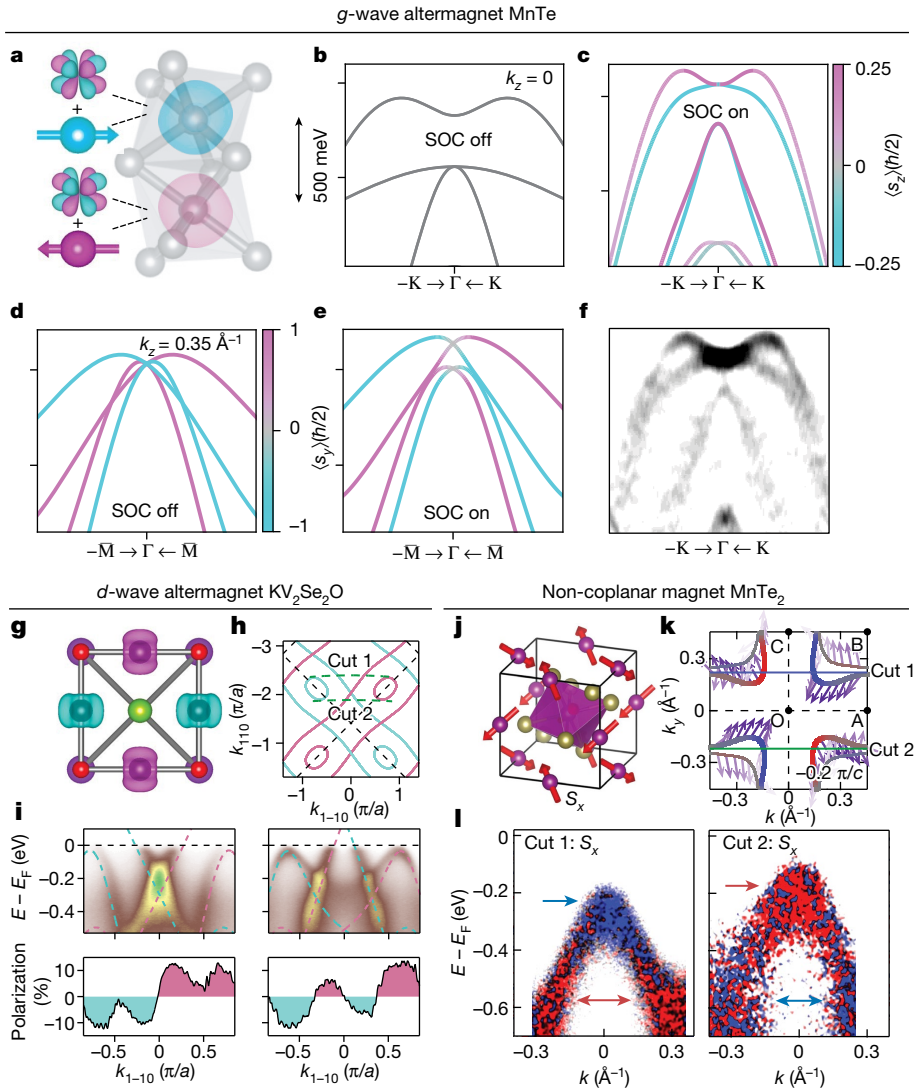

Fig. 3 | *g*-wave and *d*-wave altermagnets and a non-coplanar magnet. a, MnTe magnetic crystal structure with grey spheres representing Te atoms. Cyan and magenta local spin densities on Mn atoms inside the Te octahedra are schematically decomposed into isotropic dipole (sphere with arrow) and anisotropic *g*-wave components. Cyan and magenta colours mark opposite spin polarizations. **b**, Density functional theory (DFT) spin-polarized band structure along a $k_z = 0$ path in the Brillouin zone in the $k_z = 0$ nodal plane with the spin–orbit coupling (SOC) turned off. **c**, The same as in **b** but with SOC turned on. **d**,**e**, The same as in **b** and **c**, respectively, but along a $k_z \neq 0$ path in the Brillouin zone away from the four nodal planes of the *g*-wave altermagnetic order. s_y in panels **d**,**e** labels the in-plane spin component parallel to the Néel vector in the position space, while s_z in panel **c** labels the out-of-plane spin component orthogonal to the Néel vector. **f**, ARPES measurements of the spin-split band structure corresponding to the DFT in **c**. **g**, KV_2Se_2O magnetic crystal structure with local anisotropic spin densities on V atoms. K atoms, purple; O atoms, red; Se atoms, green. **h**, Calculated spin-resolved Fermi surface at $k_z = 0$ with green dashed lines indicating the momentum locations of cuts 1 and 2 in the Brillouin zone. **i**, ARPES intensity plots showing the band dispersion along cuts 1 and 2. Magenta and cyan dashed curves are calculated spin-up and spin-down bands. Magenta and cyan filled areas highlight the momentum-dependent spin-up and spin-down polarizations calculated by the asymmetry of the measured spin-up and spin-down signals. E and E_F denote energy and Fermi level, respectively, and $k_{[110]}$ and $k_{[1\text{-}10]}$ are in-plane momenta. **j**, Crystal structure of $MnTe_2$. The compensated non-coplanar magnetic configuration on Mn atoms is indicated by the red arrows (yellow spheres represent Te atoms forming octahedra around Mn atoms). **k**, DFT-derived, spin-resolved k_x–k_y map at 21.2 eV and at binding energy $E_B = 0.45$ eV. Magenta arrows show in-plane direction of the spin; the darkness of the arrows shows the magnitude of in-plane spin polarization; the colour of the bands shows the magnitude of the out-of-plane S_z polarization. The O–A–B–C plane is the $k_z = -0.2\pi/c$ plane. **l**, ARPES-measured, S_x-resolved cuts 1 and 2. The k positions of cuts 1 and 2 are marked in **k**. Panels adapted with permission from: **b**–**f**, ref. 97 under a Creative Commons licence CC BY 4.0; **h**,**i**, ref. 111, Springer Nature Limited; **j**–**l**, ref. 141, Springer Nature Limited.

Recently, the unconventional *T*-symmetry-breaking spin splitting in the compensated magnets was reported by angle-resolved photoemission spectroscopy (ARPES) measurements in the *g*-wave altermagnets MnTe, CrSb or $CoNb_4Se_8$ (refs. 97–100,103–109; Fig. 3a–f), and the *d*-wave altermagnets KV_2Se_2O or RbV_2Te_2O (refs. 111,112; Fig. 3g–i). Unconventional spin splitting was also experimentally observed by ARPES measurements in a non-collinear non-coplanar compensated magnet $MnTe_2$ (ref. 141; Fig. 3j–l). In contrast to the collinear altermagnetic ordering, here the non-collinear ordering generates a corresponding non-collinear spin texture in the band structure of $MnTe_2$.

Below we start with a discussion of the electronic structure of altermagnets in the limit of zero spin–orbit coupling. This is followed by a comparison with non-relativistic electronic structures of several representative magnets with compensated non-collinear spin orders. Finally, we include a discussion of relativistic and topological effects in the altermagnetic band structures.

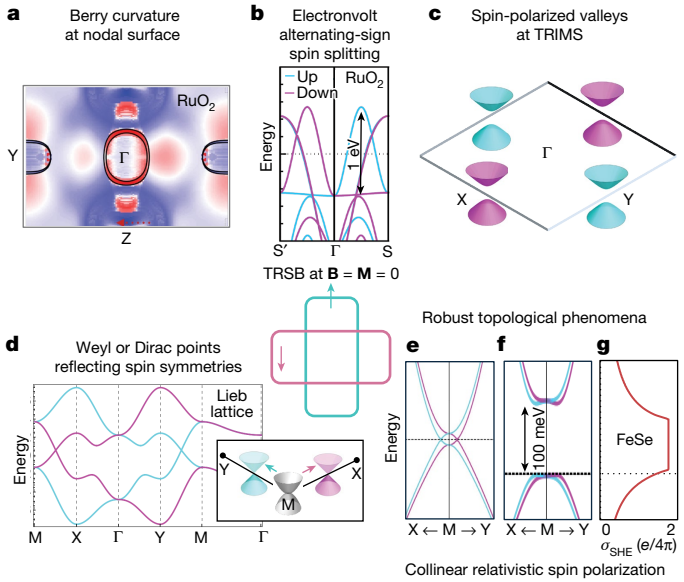

Fig. 4 | Salient electronic structure features of altermagnets. The middle panel shows *T* symmetry breaking (TRSB) in the even-parity electronic structure of altermagnets in the limit of zero spin–orbit coupling and at zero external magnetic field and internal magnetization. **a**, Berry curvature projected on the nodal surface with hotspots around the bands intersecting the nodal surface spin split by the spin–orbit coupling. **b**, Spin splitting without spin–orbit coupling with opposite sign along two perpendicular directions and magnitude reaching the electronvolt scale. DFT calculations are for the altermagnetic phase of RuO_2. **c**, Cartoon of spin-split valleys without spin–orbit coupling around *T*-invariant momenta (TRIMS)[53,54,136,138,142]. **d**, Band structure of the altermagnetic 2D Lieb-lattice model; the inset shows the emergence of symmetry-related Dirac points from the splitting of the quadratic band crossing. **e**, DFT calculation of bands without spin–orbit coupling in a *d*-wave altermagnetic phase of electrically gated 2D FeSe. **f**, Corresponding DFT calculation with spin–orbit coupling showing collinear spin polarization in a topological insulating phase. **g**, Corresponding quantum spin Hall effect with precise quantization of the spin-Hall conductivity. Panels adapted with permission from: **a**,**b**, ref. 3, AAAS; **d**, ref. 113, American Physical Society; **e**–**g**, ref. 7.

Non-relativistic spectroscopy signatures

The symmetry and microscopy signatures of altermagnetism, described in previous sections, are directly reflected in the spin-dependent band structure in the momentum space in the limit of zero relativistic spin–orbit coupling. The symmetries of the collinear spin-only group $Z_2^{C_2T} \ltimes SO(2)$, together with *T* acting in both the spin space and the real space, imply an effective *P* symmetry in the momentum space. The spin-dependent electronic structure in the momentum space for the altermagnetic order thus has the *P* symmetry, regardless of whether the magnetic crystal has or has not the *P* symmetry in the position space[1].

In total, there are ten non-trivial *P*-symmetric spin point groups (ten non-trivial spin Laue groups) of the form introduced above, $([E\|H] + [C_2\|G - H])$, describing the spin- and momentum-dependent band structures in the non-relativistic limit for all altermagnetic spin orders on crystals[1]. Apart from the spin degeneracy at the Γ point, the symmetries of a first class of altermagnets, described by four out of the ten non-trivial spin Laue groups, protect spin degeneracy at two nodal surfaces in the 3D Brillouin zone crossing the Γ point. In the second class, corresponding to another four non-trivial spin Laue groups, there are four symmetry-protected spin-degenerate nodal surfaces. A third altermagnetic class, containing the remaining two non-trivial spin Laue groups, has six spin-degenerate nodal surfaces protected by symmetry. Outside these nodal surfaces, the spin symmetries allow for lifting the spin degeneracy, resulting in even-parity *T*-symmetry-breaking electronic spectra in the three altermagnetic classes of the *d*-, *g*- or *i*-wave form, respectively[1]. The *d*-, *g*- or *i*-wave spectra in the momentum space correspond to the ferroicly ordered *d*-, *g*- or *i*-wave spin-density components in the position space of the altermagnetic crystals, discussed in the previous section[94]. We note that compared with the 10 spin Laue[1] (37/422 point[1]/space[4,57]) groups of altermagnets, there are 11 spin Laue (32/230 point/space) groups corresponding to the collinear ferromagnetic ordering with split majority-spin and minority-spin bands, and 11 spin Laue (53/769 point/space) groups of the collinear antiferromagnetic ordering with spin-degenerate bands[1,4,57].

The possibility of a strong *T*-symmetry-breaking spin polarization in the non-relativistic electronic structure away from the nodal surfaces, with spin splitting of the bands on an electronvolt scale, was pointed out in the initial theoretical studies of the altermagnetic phase of RuO_2 (refs. 3,133; Fig. 4b). Another distinctive band-structure feature in the limit of zero spin–orbit coupling, introduced in theoretical studies of several altermagnetic candidates, is the presence of spin-polarized valleys[53,54,136,138,142] (Fig. 4c). Unlike in the relativistic spectra of non-magnetic systems, the non-relativistic band structures of altermagnets can host these spin-polarized valleys at *T*-invariant momenta.

Comparison with non-collinear compensated magnets

Using the spin symmetries, we now discuss the salient features of the altermagnetic electronic structure in the limit of zero spin–orbit coupling, highlighted in Fig. 2a, in comparison with different representative non-collinear magnets with a compensated spin order protected by spin symmetry, illustrated in Fig. 2b–e. All compensated magnetic structures in Fig. 2a–e break the *PT* symmetry. Recall that the *PT* symmetry protects Kramers spin degeneracy of the electronic structure across the whole Brillouin zone, both without and with the spin–orbit coupling[143–146].

We note that non-collinear spin arrangements on crystals can originate from, for example, frustrated exchange interactions in the absence of spin–orbit coupling, or from Dzyaloshinskii–Moriya interaction. (Even in the latter case where spin–orbit coupling contributes to the stabilization of the non-collinear spin ordering, the spin-ordering symmetry can be described by spin-group symmetries).

In Fig. 2b, we show the Mn_3Sn member of the intensely studied Mn_3X family of non-collinear compensated magnets[31,67,130,147–170]. The right panel of Fig. 2b shows a cartoon of the even-parity *T*-symmetry-breaking electronic structure of Mn_3Sn whose compensated magnetic crystal breaks, besides the *PT* symmetry, also the *tT* symmetry (left panel of Fig. 2b). These momentum-space and position-space symmetry characteristics are analogous to the altermagnetic order (Fig. 2a). Unlike altermagnetism, however, the spin arrangement on the crystal in Fig. 2b is non-collinear (coplanar), resulting in a spin-dependent electronic structure with a non-collinear (coplanar) spin texture in the momentum space that winds twice along the Fermi surface[158]. Also in contrast to the anisotropic nodal altermagnetic order, and reminiscent of the nodeless ferromagnetic order, the shape of the energy isosurfaces and the spin-splitting magnitude do not show a spontaneous anisotropic deformation but preserve the symmetry of the underlying crystal lattice.

In Fig. 2d,e, we show cartoons of non-relativistic spin-dependent electronic structures having odd parity and *T* symmetry[59,60,67,171–175]. They contrast with the so far discussed even-parity *T*-symmetry-breaking spectra of collinear altermagnets and ferromagnets, and the non-collinear *P*-symmetric magnets represented by Mn_3Sn. The odd-parity *T*-symmetric type of non-relativistic spin-split spectra in the momentum space is due to the broken *P* symmetry in a non-collinear magnetic crystal structure. In addition, it is enabled by the presence of the *tT* symmetry (Fig. 2d,e). This antiferroic order, in which opposite atomic magnetic dipoles are related by translation in the crystal lattice, contrasts with the ferroic order of the local dipoles in ferromagnets, or the ferroic order of the higher even-parity-wave components of

the local spin density in altermagnets. The momentum-space electronic spectra generated by the antiferroic order of the tT-symmetric non-collinear magnets in Fig. 2d,e also contrast with the collinear Néel antiferromagnets. In the latter case, the tT symmetry together with the collinearity in the position space protects the spin degeneracy of the even-parity non-relativistic spectra in the momentum space (Fig. 2f).

Figure 2d illustrates the odd-parity magnetism on a non-collinear coplanar spin structure in the position space of the crystal. Here the tT symmetry together with the coplanar spin-only group $Z_2^{C_2T}$ results in a symmetry $[C_2||t]$, combining a real-space translation with a two-fold spin-space rotation around the axis orthogonal to the coplanar spins. This allows for a compensated magnetic phase with an odd-parity electronic energy spectrum as a function of momentum, $E_\uparrow(\mathbf{k}) = E_\downarrow(-\mathbf{k})$, and a collinear spin polarization in the momentum space with the polarization aligned along the above C_2 spin-rotation axis[59]. To highlight the combination of the tT-symmetric antiferroic order in the position space, reminiscent of the Néel antiferromagnetism, with the collinear alternating spin polarization in the momentum space, akin to altermagnetism, this type of odd-parity magnetism was recently dubbed antialtermagnetism by some of us[4].

It is noted that although the spins are collinear in the momentum space, the magnitude of their expectation value can vary with momentum. Remarkably, the spin-polarization axis of the collinear spins in the momentum space is perpendicular to the plane of the non-collinear coplanar spins in the position space of the crystal. This is to be contrasted with the case of the collinear ferromagnetic and altermagnetic ordering, for which the momentum-independent spin-quantization axis in the non-relativistic band structure is oriented along the spin axis in the crystal lattice, and where spin is a good quantum number of the electronic states.

Figure 2d illustrates a p-wave order featuring nodal spin-polarized energy isosurfaces that, compared with the normal phase, shift in opposite directions in the momentum space for opposite spin directions. This p-wave antialtermagnetism has been predicted[59] in the P-symmetry-breaking tT-symmetric non-collinear coplanar magnet CeNiAsO (ref. 59), and is expected to allow for highly efficient charge-to-spin conversion via, for example, a non-relativistic Edelstein effect[174].

Figure 2e illustrates an odd-parity electronic structure generated by a P-symmetry-breaking tT-symmetric non-coplanar spin arrangement on the crystal of Ce_3InN. Because of the absence of the coplanar symmetry $Z_2^{C_2T}$, the bands have spin textures with momentum-dependent magnitude and direction of spins[60] (A. B. Hellenes, T. J., J. S. & L. Š., manuscript in preparation). These odd-parity T-symmetric spin textures in the momentum space of the magnet represent a non-relativistic spin-ordering counterpart of the relativistic spin–orbit-coupled textures in electronic spectra of non-magnetic crystals with broken P symmetry.

Finally, in Fig. 2c, we highlight an example of a non-coplanar compensated magnetic crystal CoM_3S_6 (M = Ta or Nb) breaking both the tT and the PT symmetries. Remarkably, despite the broken tT and the PT symmetries, the non-relativistic band structure has a symmetry-protected spin degeneracy across the whole Brillouin zone[64,67,132,151]. This contrasts with the spin-split non-relativistic band structures of altermagnets (Fig. 2a), the class of non-collinear compensated magnets represented in Fig. 2b by Mn_3Sn, or the conventional uncompensated ferromagnets, all also sharing the broken tT and PT symmetries. The spin degeneracy of the electronic spectrum of CoM_3S_6, illustrated in Fig. 2c, is protected by multiple symmetry elements in the spin space group combining a real-space translation with a spin-space rotation[64,67,132].

We recall that the tT and PT symmetry-breaking compensated magnetic orders with spin-split non-relativistic electronic spectra, represented in Fig. 2a,b, can generate (in the presence of the spin–orbit coupling) the anomalous Hall effect[3,53,55,75,102,130,147–150,176–179]. The spin ordering in the non-coplanar compensated magnet CoM_3S_6, illustrated in Fig. 2c, also breaks the tT and PT symmetry and allows for the anomalous Hall effect (even in the absence of the spin–orbit coupling), whereas the non-relativistic electronic spectrum is spin degenerate[67,151]. Vice versa, Fig. 2d,e shows examples of non-collinear compensated spin orders with the tT symmetry and broken PT symmetry whose non-relativistic band structure is spin split while the anomalous Hall effect is excluded by symmetry (without or with the spin–orbit coupling)[59]. Finally, in the collinear Néel antiferromagnet with the tT symmetry and PT symmetry[117], illustrated in Fig. 2f, both the spin splitting and the anomalous Hall effect (without or with the spin–orbit coupling) are excluded by symmetry.

Spin–orbit coupling and topological phenomena

We now focus on spin–orbit coupling and topological phenomena in the electronic structure of altermagnets[7,10,12,17,97,106,107,113,121,125,180–187]. The spin degeneracy at the nodal surfaces in the non-relativistic band structure of altermagnets can be lifted by the relativistic spin–orbit coupling. Among a range of phenomena further discussed in this section, this can generate Berry-curvature hotspots (Fig. 4a) and, correspondingly, large values of the anomalous Hall effect. This was initially theoretically predicted in altermagnetic candidates RuO_2 (ref. 3) or $FeSb_2$ (ref. 52), and reviewed in detail in ref. 31.

In the following paragraphs, we first give an example of the interplay of the spin–orbit coupling with the altermagnetic ordering on electronic energy bands of the 3D altermagnet MnTe and a 2D altermagnet FeSe (refs. 7,97). The feature that we highlight is a possibility to realize in altermagnets spin–orbit-coupled band structures in which the spin-polarization axis is momentum independent across high-symmetry directions, planes or the entire Brillouin zone. This is extraordinary given the general form, proportional to $\mathbf{s}\cdot(\mathbf{k}\times\mathbf{E})$, of the spin–orbit-coupling term in the Dirac equation, where $\mathbf{s}$ denotes spin, $\mathbf{k}$ denotes momentum and $\mathbf{E}$ denotes electric field. The coupling between spin and momentum vectors implies the tendency to form spin textures in the electronic structure where the magnitude and direction of spin varies with momentum, as frequently observed in ferromagnets or (P symmetry breaking) non-magnetic materials.

We contrast these spin textures with the effect of the spin–orbit coupling on the $k_z = 0$ nodal plane in altermagnetic MnTe. This material has a spin-polarized band structure without spin–orbit coupling of the nodal g-wave type, thus showing four nodal planes crossing the Γ point[1]. The spin degeneracy, protected at the nodal planes by the symmetry of the non-trivial spin point group ${}^26/{}^2m^2m^1m$, can be lifted by the spin–orbit coupling[97]. Remarkably, the spin–orbit coupling can spin-split the bands despite the P symmetry of altermagnetic MnTe. This already indicates the distinct phenomenology of spin–orbit-coupling effects in altermagnets, compared with conventional spin splitting by the spin–orbit coupling, which requires broken P symmetry.

When the Néel vector in MnTe is in the magnetic easy plane (the c plane of the MnTe crystal shown in Fig. 3a), the strong g-wave order without spin–orbit coupling generates a corresponding in-plane spin-polarization component along the Néel vector away from the nodal planes. This is complemented on the $k_z = 0$ nodal plane by an out-of-plane spin polarization of the spin–orbit-coupled bands, whose sign alternates and the polarization axis is independent of the in-plane momentum[97] (Fig. 3b–d). We point out that the absence of a momentum-dependent non-collinear spin texture on the $k_z = 0$ plane is realized at energies in the band structure with a strong admixture of orbitals from the heavy element Te. Indeed the spin splitting in this part of the spin–orbit-coupled band structure reaches large magnitudes on the scale of 100 meV (Fig. 3c,f).

The realization of such a common momentum-independent spin-polarization axis has been a long-sought goal in the research of spin–orbit-coupling band-structure effects. Besides altermagnets, this was only considered in odd-parity spectra of non-magnetic non-centrosymmetric systems. Here in 3D, the effect was attributed to (approximate)

symmetry protection in a vicinity of high-symmetry points of the Brillouin zone[188]. In 2D, it was predicted to occur owing to the presence of a mirror symmetry[189], or was observed for fine-tuned strengths of microscopic Rashba and Dresselhaus spin–orbit coupling[190,191].

In altermagnetic MnTe, the collinear spin-polarization on the $k_z = 0$ nodal plane, with all spins pointing along the normal to the plane, is observed in even-parity spectra and is symmetry protected[97]. Specifically, the absence of any in-plane spin-polarization component on the $k_z = 0$ nodal plane is enforced by the mirror symmetry of the magnetic point group $m'm'm$, where the mirror plane is parallel to the crystal c plane. An analogous effect was predicted in a supercell structure based on altermagnetic $LaMnO_3$ (ref. 189).

We emphasize that the $m'm'm$ magnetic-group symmetry is only present in MnTe for the Néel vector oriented along the c plane in the crystal[97]. In contrast, in the g-wave altermagnet CrSb, which has identical crystallographic and spin groups as MnTe (ref. 1), the spin–orbit coupling leads to the Néel vector easy axis pointing along the crystal c axis. It changes the magnetic point group to $6'/m'mm'$ with a symmetry combining the c-plane mirror with T in CrSb. This CrSb symmetry does not enforce the absence of the in-plane spin-polarization component in the $k_z = 0$ plane; instead it enforces the absence of the out-of-plane spin-polarization component for states with momenta along the $k_x = k_y = 0$ line (which turns out to be a completely spin-degenerate nodal line because of the interplay with another magnetic-group mirror symmetry)[121].

An additional extraordinary feature of the spin–orbit coupling in the MnTe altermagnet with in-plane Néel vector is a quadratic band dispersion and spin splitting near the Γ point (Fig. 3c,f). The absence of the constant and linear spin-splitting terms highlights the principal distinction from the exchange spin splitting present in ferromagnets and the spin–orbit-coupling-induced spin splitting present in the non-magnetic P-symmetry-breaking crystals.

The collinear spin polarization is not a feature seen exclusively in the spin–orbit-coupled band structure of MnTe. In Fig. 4e,f, we show the electronic structure of a candidate 2D altermagnet FeSe (ref. 7). Without spin–orbit coupling (Fig. 4e), the spin-polarized 2D bands have a d-wave ordering. When spin–orbit coupling is included and the Néel vector is oriented in the direction normal to the 2D plane (Fig. 4f), spin-polarized states in valleys around M points in the Brillouin zone acquire a common spin axis, this time parallel to the Néel vector. For energy ranges where the spectrum contains only the M-point valleys, the entire energy isosurface in the 2D momentum space has a common momentum-independent spin-polarization axis. This is again despite the large spin–orbit-coupling strength introduced by Se, which generates a splitting in the M-point valleys on the 100-meV scale (Fig. 4f).

We now move on to topological phenomena. In the non-collinear compensated magnets, the observation of the large anomalous Hall effect prompted the research of Weyl fermions and topological signatures in the magnetotransport[132,151,192–195]. Below we highlight topological band-structure phenomena that are characteristic of altermagnets[7,9,10,12,17,106,107,113,121,125,181–187,196]. Several of these phenomena are related to the spin-degenerate nodal lines in the Brillouin zone, which are the remnants of the nodal planes of the altermagnet when the spin–orbit coupling is included. They are topologically trivial with respect to non-spatial symmetries. When present, however, these Brillouin-zone nodal lines, and the corresponding Weyl nodes in the band structure, can be protected by mirror symmetries of the crystal[121,183,184]. Therefore, they remain stable against small perturbations (for example, by magnetic field or strain) that preserve the mirror symmetries[121].

We again illustrate these and other topological phenomena on representative altermagnetic materials. In CrSb, the splitting of the $k_z = 0$ nodal plane by the spin–orbit coupling leads to the emergence of pairs of Weyl points and thus Fermi surface arcs[106]. Here the Weyl points result from the crossing of bands with opposite spin. Conversely, along the spin-split parts of the Brillouin zone in the band structure without spin–orbit coupling, crossings of bands with the same spin give rise to spin-polarized Weyl points. Fermi arcs connecting the surface projections of the Weyl points with the same total spin are also spin polarized[106,107]. In altermagnetic VNb_3S_6, signatures of linearly dispersing Weyl nodes were experimentally detected by Raman scattering spectroscopy[196].

An extraordinary interplay of topology and spin–orbit coupling can be illustrated on the 2D altermagnetic candidate FeSe (ref. 7; Fig. 4e–g). Without spin–orbit coupling, the bands feature spin degeneracy above and below the Fermi level at the M points, which are located at the two nodal lines in the 2D Brillouin zone of this d-wave altermagnet (Fig. 4e). In addition, there are two crossings of bands with the same spin at the Fermi level. They are located on the M–X and M–Y lines (Fig. 4e), respectively, and are connected by the altermagnetic spin symmetries. Spin–orbit coupling splits these same-spin band crossings and shifts further apart in energy the two spin-degenerate bands at the M point by about 100 meV, resulting in the formation of a 2D topological spin-Chern insulator (Fig. 4f). As already highlighted above in the discussion of the spin–orbit-coupling effects in FeSe, the spin polarization maintains a momentum-independent axis in the valleys around the M points, even for this relatively large strength of the spin–orbit coupling in FeSe. This leads to an exceptionally precise quantization of the quantum spin Hall effect over a broad range of energies[7] (Fig. 4g).

Crossings of bands with the same spin, and their connection to non-trivial topology, are widespread in altermagnetic materials[113,125,186]. Further insights about the topological nature of such crossings follow from analysing the 2D Lieb-lattice model[7,8,113,114] (Fig. 1), of which monolayer FeSe is a particular material realization. A characteristic feature of this model, illustrated in Fig. 4d, is the existence of a quadratic band crossing at the M point[197]. Altermagnetic order splits the quadratic band crossing into pairs of crossings of same-spin bands (Dirac points in 2D) located at the M–X and M–Y zone edges and related by the $[C_2||C_4]$ spin symmetry (see inset of Fig. 4d). Although these Dirac points are guaranteed to exist for an infinitesimally small sublattice magnetic moment, a large enough moment will bring the Dirac crossings to the X and Y points and remove them. The impact of the spin–orbit coupling depends on the direction of the Néel vector[113]. For the out-of-plane direction, like in the case of the above discussed FeSe, the Dirac points are gapped out, resulting in the topological quantum spin Hall state and mirror spin-Chern bands.[7,113]. For the in-plane Néel vector, however, even if the Dirac points are gapped, the bands are topologically trivial. This illustrates that the direction of the Néel vector has a substantial impact on the opposite-spin and same-spin band crossings. In 3D lattices, same-spin band crossings can also occur, where they can give rise to Weyl nodal loops in the presence of spin–orbit coupling[113].

Another promising route to imprint unusual electronic properties in altermagnetic materials is to combine their characteristic anisotropic nodal spin ordering with other phases, such as quantum anomalous Hall Chern insulators, axion insulators, multiferroics or superconductors[1,2,5–30]. The interplay between superconductivity and altermagnetism or altermagnetic fluctuations has been investigated as intrinsic phenomena in a single material or in the context of heterostructures, where pairing is induced by the proximity effect, and bulk systems, where pairing and altermagnetic ordering coexist. These studies have revealed the emergence of intriguing phenomena, such as unconventional Andreev reflection, pair density waves, non-trivial topological modes and non-reciprocal supercurrents.

Outlook

The salient band-structure features of altermagnets can have unparalleled practical utility in spintronics, sharing the merits of the vanishing net magnetization with the earlier studied collinear and non-collinear compensated magnets, and sharing the merits of the well-separated

and conserved spin-up and spin-down channels with the conventional ferromagnets.

Altermagnetism can lead to unique spin–orbit coupling and topological phenomena, such as spin polarizations that are collinear despite their spin–orbit-coupling origin, or topological Weyl points that reflect the specific altermagnetic spin-group symmetries. In addition, altermagnets represent a unique platform to search for quantized topological responses at zero magnetic field and high temperatures, or to combine this anisotropic compensated *T*-symmetry-breaking magnetic ordering with superconductivity.

Notwithstanding the remarkable and rapid progress in the field, several open questions remain and new research directions emerge on the horizon. For instance, it is an intriguing question whether an altermagnetic quantum critical point can promote new phenomena[179,198], perhaps related to non-Fermi liquid behaviour and unconventional superconductivity, that is not encountered in other widely studied quantum-critical ferroic orders, such as ferromagnetism, ferroelectricity and nematicity. A recent report on the coexistence of the strange metallic behaviour and the anomalous Hall effect in an altermagnetic phase of a Kondo lattice-like flat-band system[179] illustrates the emergence of a research path exploring the impact of correlations and bad metal behaviour on altermagnetic properties of strongly correlated materials.

Finally, an extensive experimental effort, complementing the parallel fruitful research of other compensated magnetic phases, is needed to establish all the predicted specific symmetry, microscopy and spectroscopy signatures of altermagnetism, to further explore the corresponding unconventional electronic and optical responses, and to exploit them in novel devices.

1. Šmejkal, L., Sinova, J. & Jungwirth, T. Beyond conventional ferromagnetism and antiferromagnetism: a phase with nonrelativistic spin and crystal rotation symmetry. *Phys. Rev. X* **12**, 031042 (2022).
This paper delineated altermagnetism as an exclusively distinct spin-group symmetry class of *d*-, *g*- or *i*-wave spin-ordered phases.
2. Šmejkal, L., Sinova, J. & Jungwirth, T. Emerging research landscape of altermagnetism. *Phys. Rev. X* **12**, 040501 (2022).
This perspective outlined envisaged research directions of altermagnetism.
3. Šmejkal, L., González-Hernández, R., Jungwirth, T. & Sinova, J. Crystal time-reversal symmetry breaking and spontaneous Hall effect in collinear antiferromagnets. *Sci. Adv.* **6**, eaaz8809 (2020).
This paper predicted that an interplay of crystal and collinear spin orders in a class of materials can lead to a time-reversal-symmetry-breaking spin-split electronic structure and, when spin–orbit coupling is included, to the anomalous Hall effect.
4. Jungwirth, T. et al. Altermagnetism: an unconventional spin-ordered phase of matter. *Newton* **1**, 100162 (2025).
5. Mazin, I. I. Notes on altermagnetism and superconductivity. *AAPPS Bull.* **35**, 18 (2025).
These informal notes, originally posted as a preprint on the arXiv server, aimed to stimulate the exploration of the interplay of altermagnetism with superconductivity.
6. Beenakker, C. W. J. & Vakhtel, T. Phase-shifted Andreev levels in an altermagnet Josephson junction. *Phys. Rev. B* **108**, 075425 (2023).
7. Mazin, I., González-Hernández, R. & Šmejkal, L. Induced monolayer altermagnetism in $MnP(S,Se)_3$ and FeSe. Preprint at http://arxiv.org/abs/2309.02355 (2023).
8. Brekke, B., Brataas, A. & Sudbø, A. Two-dimensional altermagnets: superconductivity in a minimal microscopic model. *Phys. Rev. B* **108**, 224421 (2023).
9. Li, Y.-X. & Liu, C.-C. Majorana corner modes and tunable patterns in an altermagnet heterostructure. *Phys. Rev. B* **108**, 205410 (2023).
10. Zhu, D., Zhuang, Z.-Y., Wu, Z. & Yan, Z. Topological superconductivity in two-dimensional altermagnetic metals. *Phys. Rev. B* **108**, 184505 (2023).
11. Sumita, S., Naka, M. & Seo, H. Fulde–Ferrell–Larkin–Ovchinnikov state induced by antiferromagnetic order in k-type organic conductors. *Phys. Rev. Res.* **5**, 043171 (2023).
12. Ghorashi, S. A. A., Hughes, T. L. & Cano, J. Altermagnetic routes to Majorana modes in zero net magnetization. *Phys. Rev. Lett.* **133**, 106601 (2024).
13. Papaj, M. Andreev reflection at the altermagnet-superconductor interface. *Phys. Rev. B* **108**, L060508 (2023).
14. Wei, M. et al. Gapless superconducting state and mirage gap in altermagnets. *Phys. Rev. B* **109**, L201404 (2023).
15. Zhang, S.-B., Hu, L.-H. & Neupert, T. Finite-momentum Cooper pairing in proximitized altermagnets. *Nat. Commun.* **15**, 1801 (2024).
16. Cheng, Q. & Sun, Q.-F. Orientation-dependent Josephson effect in spin-singlet superconductor/altermagnet/spin-triplet superconductor junctions. *Phys. Rev. B* **109**, 024517 (2024).
17. Zhao, Y. et al. Hybrid-order topology in unconventional magnets of Eu-based Zintl compounds with surface-dependent quantum geometry. *Phys. Rev. B* **110**, 205111 (2024).
18. Mæland, K., Brekke, B. & Sudbø, A. Many-body effects on superconductivity mediated by double-magnon processes in altermagnets. *Phys. Rev. B* **109**, 134515 (2024).
19. Chakraborty, D. & Black-Schaffer, A. M. Zero-field finite-momentum and field-induced superconductivity in altermagnets. *Phys. Rev. B* **110**, L060508 (2024).
20. Banerjee, S. & Scheurer, M. S. Altermagnetic superconducting diode effect. *Phys. Rev. B* **110**, 024503 (2024).
21. Jeschke, H. O., Shimizu, M. & Mazin, I. I. $CuAg(SO_4)_2$: a doubly strongly correlated altermagnetic three-dimensional analog of the parent compounds of high-T_c cuprates. *Phys. Rev. B* **109**, L220412 (2024).
22. Verbeek, X. H., Urru, A. & Spaldin, N. A. Hidden orders and (anti-)magnetoelectric effects in Cr_2O_3 and Fe_2O_3. *Phys. Rev. Res.* **5**, L042018 (2023).
23. Bernardini, F., Fiebig, M. & Cano, A. Ruddlesden–Popper and perovskite phases as a material platform for altermagnetism. *J. Appl. Phys.* **137**, 103903 (2025).
24. Zyuzin, A. A. Magnetoelectric effect in superconductors with *d*-wave magnetization. *Phys. Rev. B* **109**, L220505 (2024).
25. Sim, G. & Knolle, J. Pair density waves and supercurrent diode effect in altermagnets. *Phys. Rev. B* **112**, L020502 (2025).
26. Hu, J.-X., Matsyshyn, O. & Song, J. C. W. Nonlinear superconducting magnetoelectric effect. *Phys. Rev. Lett.* **134**, 026001 (2025).
27. Šmejkal, L. Altermagnetic multiferroics and altermagnetoelectric effect. Preprint at http://arxiv.org/abs/2411.19928 (2024).
This paper and refs. 28 and 29 theoretically predicted an interplay of altermagnetism with ferroelectricity.
28. Duan, X. et al. Antiferroelectric altermagnets: antiferroelectricity alters magnets. *Phys. Rev. Lett.* **134**, 106801 (2025).
29. Gu, M. et al. Ferroelectric switchable altermagnetism. *Phys. Rev. Lett.* **134**, 106802 (2024).
30. Parthenios, N. et al. Spin and pair density waves in two-dimensional altermagnetic metals. *Phys. Rev. B* **112**, 214410 (2025).
31. Šmejkal, L., MacDonald, A. H., Sinova, J., Nakatsuji, S. & Jungwirth, T. Anomalous Hall antiferromagnets. *Nat. Rev. Mater.* **7**, 482–496 (2022).
This paper reviewed the anomalous Hall effect in altermagnets and non-collinear compensated magnets.
32. Bai, L. et al. Altermagnetism: exploring new frontiers in magnetism and spintronics. *Adv. Funct. Mater.* **34**, 2409327 (2024).
33. Liu, Q., Dai, X. & Blügel, S. Different facets of unconventional magnetism. *Nat. Phys.* **21**, 329–331 (2025).
34. Song, C. et al. Altermagnets as a new class of functional materials. *Nat. Rev. Mater.* **10**, 473–485 (2025).
35. Jungwirth, T. et al. Altermagnetic spintronics. Preprint at http://arxiv.org/abs/2508.09748 (2025).
36. Liu, P., Li, J., Han, J., Wan, X. & Liu, Q. Spin-group symmetry in magnetic materials with negligible spin–orbit coupling. *Phys. Rev. X* **12**, 21016 (2022).
This paper discusses spin space-group symmetries of magnetic materials and corresponding band degeneracies and emergent topological phases.
37. Litvin, D. B. & Opechowski, W. Spin groups. *Physica* **76**, 538–554 (1974).
This paper describes the mathematical spin-group formalism.
38. Andreev, A. & Grishchuk, I. Spin nematics. *Sov. Phys. JETP* **60**, 267 (1984).
39. Gor'kov, L. P. & Sokol, A. Nontrivial magnetic order: localized versus itinerant systems. *Phys. Rev. Lett.* **69**, 2586–2589 (1992).
40. Leggett, A. J. Nobel Lecture: Superfluid 3-He: the early days as seen by a theorist. *Rev. Mod. Phys.* **76**, 999 (2004).
This paper reviews the superfluid phase of ^{3}He, including the spontaneous breaking of real-space and spin-space rotation symmetries.
41. Moessner, R. & Moore, J. E. *Topological Phases of Matter* (Cambridge Univ. Press, 2021).
42. Strange, P. *Relativistic Quantum Mechanics* 1 edn (Cambridge Univ. Press, Cambridge, 1998).
43. Winkler, R. *Spin–Orbit Coupling Effects in Two-Dimensional Electron and Hole Systems* Springer Tracts in Modern Physics Vol. 191 (Springer, 2003).
44. Landau, L. & Lifshitz, E. *Electrodynamics of Continuous Media* 2 edn, Course of Theoretical Physics Vol. 8 (Pergamon Press, 1965).
45. Sinova, J., Valenzuela, S. O., Wunderlich, J., Back, C. H. & Jungwirth, T. Spin Hall effects. *Rev. Mod. Phys.* **87**, 1213–1260 (2015).
46. Nagaosa, N., Sinova, J., Onoda, S., MacDonald, A. H. & Ong, N. P. Anomalous Hall effect. *Rev. Mod. Phys.* **82**, 1539–1592 (2010).
47. Franz, M. & Molenkamp, L. (eds) *Contemporary Concepts of Condensed Matter Science* Topological Insulators Vol. 6 (Elsevier, 2013).
48. Murakami, S. & Yokoyama, T. *Quantum Spin Hall Effect and Topological Insulators* Vol. 1 (Oxford Univ. Press, 2017).
49. Bradlyn, B. et al. Topological quantum chemistry. *Nature* **547**, 298–305 (2017).
50. Armitage, N. P., Mele, E. J. & Vishwanath, A. Weyl and Dirac semimetals in three-dimensional solids. *Rev. Mod. Phys.* **90**, 015001 (2018).
51. Elcoro, L. et al. Magnetic topological quantum chemistry. *Nat. Commun.* **12**, 5965 (2021).
52. Mazin, I. I., Koepernik, K., Johannes, M. D., González-Hernández, R. & Šmejkal, L. Prediction of unconventional magnetism in doped $FeSb_2$. *Proc. Natl Acad. Sci. USA* **118**, e2108924118 (2021).
53. Reichlova, H. et al. Observation of a spontaneous anomalous Hall response in the Mn_5Si *d*-wave altermagnet candidate. *Nat. Commun.* **15**, 4961 (2024).
54. Šmejkal, L., Hellenes, A. B., González-Hernández, R., Sinova, J. & Jungwirth, T. Giant and tunneling magnetoresistance in unconventional collinear antiferromagnets with nonrelativistic spin–momentum coupling. *Phys. Rev. X* **12**, 011028 (2022).
55. Gonzalez Betancourt, R. D. et al. Spontaneous anomalous Hall effect arising from an unconventional compensated magnetic phase in a semiconductor. *Phys. Rev. Lett.* **130**, 036702 (2023).
56. Šmejkal, L. et al. Chiral magnons in altermagnetic RuO_2. *Phys. Rev. Lett.* **131**, 256703 (2023).
57. Chen, X. et al. Unconventional magnons in collinear magnets dictated by spin space groups. *Nature* **640**, 349–354 (2025).
58. Hariki, A. et al. X-ray magnetic circular dichroism in altermagnetic α-MnTe. *Phys. Rev. Lett.* **132**, 176701 (2024).

59. Hellenes, A. B. et al. *P*-wave magnets. Preprint at http://arxiv.org/abs/2309.01607 (2023).
60. Hellenes, A. B., Jungwirth, T., Sinova, J. & Šmejkal, L. Exchange spin–orbit coupling and unconventional *p*-wave magnetism. Preprint at http://arxiv.org/abs/2309.01607v1 (2023).
61. McClarty, P. A. & Rau, J. G. Landau theory of altermagnetism. *Phys. Rev. Lett.* **132**, 176702 (2023).
62. Smolyanyuk, A., Šmejkal, L. & Mazin, I. I. A tool to check whether a symmetry-compensated collinear magnetic material is antiferro- or altermagnetic. *SciPost Phys. Codebases* **30**, 1–16 (2024).
63. Shinohara, K. et al. Algorithm for spin symmetry operation search. *Acta Crystallogr. A* **80**, 94–103 (2024).
64. Watanabe, H., Shinohara, K., Nomoto, T., Togo, A. & Arita, R. Symmetry analysis with spin crystallographic groups: disentangling effects free of spin–orbit coupling in emergent electromagnetism. *Phys. Rev. B* **109**, 094438 (2024).
65. Jiang, Y. et al. Enumeration of spin-space groups: toward a complete description of symmetries of magnetic orders. *Phys. Rev. X* **14**, 031039 (2024).
66. Zhu, H., Li, J., Chen, X., Yu, Y. & Liu, Q. Magnetic geometry induced quantum geometry and nonlinear transports. *Nat. Commun.* **16**, 4882 (2025).
67. Chen, X. et al. Enumeration and representation theory of spin space groups. *Phys. Rev. X* **14**, 031038 (2024).
68. Schiff, H., Corticelli, A., Guerreiro, A., Romhányi, J. & McClarty, P. The crystallographic spin point groups and their representations. *SciPost Phys.* **18**, 109 (2025).
69. Xiao, Z., Zhao, J., Li, Y., Shindou, R. & Song, Z.-D. Spin space groups: full classification and applications. *Phys. Rev. X* **14**, 031037 (2024).
70. Litvin, D. B. *Magnetic Group Tables* (IUCr, 2013). http://www.iucr.org/publ/978-0-9553602-2-0.
71. Berlijn, T. et al. Itinerant antiferromagnetism in RuO_2. *Phys. Rev. Lett.* **118**, 077201 (2017).
72. Zhu, Z. H. et al. Anomalous antiferromagnetism in metallic RuO_2 determined by resonant X-ray scattering. *Phys. Rev. Lett.* **122**, 017202 (2019).
73. Lovesey, S. W., Khalyavin, D. D. & van der Laan, G. Magnetic properties of RuO_2 and charge-magnetic interference in Bragg diffraction of circularly polarized X-rays. *Phys. Rev. B* **105**, 014403 (2022).
74. Occhialini, C. A. et al. Local electronic structure of rutile RuO_2. *Phys. Rev. Res.* **3**, 033214 (2021).
75. Feng, Z. et al. An anomalous Hall effect in altermagnetic ruthenium dioxide. *Nat. Electron.* **5**, 735–743 (2022).
76. Bose, A. et al. Tilted spin current generated by the collinear antiferromagnet ruthenium dioxide. *Nat. Electron.* **5**, 267–274 (2022).
77. Bai, H. et al. Observation of spin splitting torque in a collinear antiferromagnet RuO_2. *Phys. Rev. Lett.* **128**, 197202 (2022).
78. Karube, S. et al. Observation of spin-splitter torque in collinear antiferromagnetic RuO_2. *Phys. Rev. Lett.* **129**, 137201 (2022).
79. Lovesey, S. W., Khalyavin, D. D. & van der Laan, G. Magnetic structure of RuO_2 in view of altermagnetism. *Phys. Rev. B* **108**, L121103 (2023).
80. Liu, Y. et al. Inverse altermagnetic spin splitting effect-induced terahertz emission in RuO_2. *Adv. Opt. Mater.* **11**, 2300177 (2023).
81. Fedchenko, O. et al. Observation of time-reversal symmetry breaking in the band structure of altermagnetic RuO_2. *Sci. Adv.* **10**, 31 (2024).
82. Smolyanyuk, A., Mazin, I. I., Garcia-Gassull, L. & Valentí, R. Fragility of the magnetic order in the prototypical altermagnet RuO_2. *Phys. Rev. B* **109**, 134424 (2024).
83. Lin, Z. et al. Observation of giant spin splitting and *d*-wave spin texture in room temperature altermagnet RuO_2. Preprint at http://arxiv.org/abs/2402.04995 (2024).
84. Keßler, P. et al. Absence of magnetic order in RuO_2: insights from μSR spectroscopy and neutron diffraction. *npj Spintronics* **2**, 50 (2024).
85. Li, Z. et al. Fully field-free spin-orbit torque switching induced by spin splitting effect in altermagnetic RuO_2. *Adv. Mater.* **37**, 2416712 (2025).
86. Wenzel, M. et al. Fermi-liquid behavior of nonaltermagnetic RuO_2. *Phys. Rev. B* **111**, L041115 (2025).
87. Jeong, S. G. et al. Altermagnetic polar metallic phase in ultra-thin epitaxially-strained RuO_2 films. Preprint at http://arxiv.org/abs/2405.05838 (2024).
88. Hiraishi, M. et al. Nonmagnetic ground state in RuO_2 revealed by muon spin rotation. *Phys. Rev. Lett.* **132**, 166702 (2024).
89. López-Moreno, S., Romero, A. H., Mejía-López, J. & Muñoz, A. First-principles study of pressure-induced structural phase transitions in MnF_2. *Phys. Chem. Chem. Phys.* **18**, 33250–33263 (2016).
This paper reported density-functional-theory calculations of non-relativistic band structure of MnF_2.
90. Noda, Y., Ohno, K. & Nakamura, S. Momentum-dependent band spin splitting in semiconducting MnO_2: a density functional calculation. *Phys. Chem. Chem. Phys.* **18**, 13294–13303 (2016).
91. Hayami, S., Yanagi, Y. & Kusunose, H. Momentum-dependent spin splitting by collinear antiferromagnetic ordering. *J. Phys. Soc. Jpn* **88**, 123702 (2019).
92. Yuan, L.-D., Wang, Z., Luo, J.-W., Rashba, E. I. & Zunger, A. Giant momentum-dependent spin splitting in centrosymmetric low-*Z* antiferromagnets. *Phys. Rev. B* **102**, 014422 (2020).
93. Bhowal, S. & Spaldin, N. A. Ferroically ordered magnetic octupoles in *d*-wave altermagnets. *Phys. Rev. X* **14**, 011019 (2024).
94. Jaeschke-Ubiergo, R. et al. Atomic altermagnetism. Preprint at https://arxiv.org/pdf/2503.10797 (2025).
95. Lovesey, S. W., Khalyavin, D. D. & van der Laan, G. Templates for magnetic symmetry and altermagnetism in hexagonal MnTe. *Phys. Rev. B* **108**, 174437 (2023).
96. Mazin, I. I. Altermagnetism in MnTe: origin, predicted manifestations, and routes to detwinning. *Phys. Rev. B* **107**, L100418 (2023).
97. Krempaský, J. et al. Altermagnetic lifting of Kramers spin degeneracy. *Nature* **626**, 517–522 (2024).
This paper and refs. 99–101 reported experimental spectroscopic observations of a *g*-wave altermagnetic band structure of MnTe.
98. Lee, S. S. et al. Broken Kramers degeneracy in altermagnetic MnTe. *Phys. Rev. Lett.* **132**, 036702 (2024).
99. Osumi, T. et al. Observation of a giant band splitting in altermagnetic MnTe. *Phys. Rev. B* **109**, 115102 (2024).
100. Hajlaoui, M. et al. Temperature dependence of relativistic valence band splitting induced by an altermagnetic phase transition. *Adv. Mater.* **36**, 2314076 (2024).
101. Aoyama, T. & Ohgushi, K. Piezomagnetic properties in altermagnetic MnTe. *Phys. Rev. Mater.* **8**, L041402 (2024).
102. Kluczyk, K. P. et al. Coexistence of anomalous Hall effect and weak magnetization in a nominally collinear antiferromagnet MnTe. *Phys. Rev. B* **110**, 155201 (2024).
103. Reimers, S. et al. Direct observation of altermagnetic band splitting in CrSb thin films. *Nat. Commun.* **15**, 2116 (2024).
104. Yang, G. et al. Three-dimensional mapping of the altermagnetic spin splitting in CrSb. *Nat. Commun.* **16**, 1442 (2025).
105. Ding, J. et al. Large band splitting in *g*-wave altermagnet CrSb. *Phys. Rev. Lett.* **133**, 206401 (2024).
106. Li, C. et al. Topological Weyl altermagnetism in CrSb. *Commun. Phys.* **8**, 311 (2025).
107. Lu, W. et al. Signature of topological surface bands in altermagnetic Weyl semimetal CrSb. *Nano Lett.* **25**, 7343–7350 (2025).
108. Zeng, M. et al. Observation of spin splitting in room-temperature metallic antiferromagnet CrSb. *Adv. Sci.* **11**, 2406529 (2024).
109. Dale, N. et al. Non-relativistic spin splitting above and below the Fermi level in a *g*-wave altermagnet. Preprint at http://arxiv.org/abs/2411.18761 (2024).
110. Liu, Z., Ozeki, M., Asai, S., Itoh, S. & Masuda, T. Chiral-split magnon in altermagnetic MnTe. *Phys. Rev. Lett.* **133**, 156702 (2024).
111. Jiang, B. et al. A metallic room-temperature *d*-wave altermagnet. *Nat. Phys.* **21**, 754–759 (2025).
This paper and ref. 113 reported experimental spectroscopic observations of a *d*-wave altermagnetic band structure.
112. Zhang, F. et al. Crystal-symmetry-paired spin–valley locking in a layered room-temperature metallic altermagnet candidate. *Nat. Phys.* **21**, 760–767 (2025).
113. Antonenko, D. S., Fernandes, R. M. & Venderbos, J. W. F. Mirror Chern bands and Weyl nodal loops in altermagnets. *Phys. Rev. Lett.* **134**, 096703 (2025).
This paper reported a theoretical study of topological phenomena in 2D (Lieb lattice) and 3D minimal models of altermagnetism.
114. Kaushal, N. & Franz, M. Altermagnetism in modified Lieb lattice Hubbard model. *Phys. Rev. Lett.* **135**, 156502 (2025).
115. Wei, C. C. et al. $La_2O_3Mn_2Se_2$: a correlated insulating layered *d*-wave altermagnet. *Phys. Rev. Mater.* **9**, 24402 (2025).
116. Maharaj, D. D. et al. Octupolar versus Néel order in cubic $5d^2$ double perovskites. *Phys. Rev. Lett.* **124**, 87206 (2020).
117. Néel, L. Magnetism and local molecular field. *Science* **174**, 985–992 (1971).
118. Chakraborty, A., González Hernández, R., Šmejkal, L. & Sinova, J. Strain-induced phase transition from antiferromagnet to altermagnet. *Phys. Rev. B* **109**, 144421 (2024).
119. Liu, Y., Yu, J. & Liu, C.-C. Twisted magnetic van der Waals bilayers: an ideal platform for altermagnetism. *Phys. Rev. Lett.* **133**, 206702 (2024).
120. Leeb, V., Mook, A., Šmejkal, L. & Knolle, J. Spontaneous formation of altermagnetism from orbital ordering. *Phys. Rev. Lett.* **132**, 236701 (2024).
121. Fernandes, R. M., de Carvalho, V. S., Birol, T. & Pereira, R. G. Topological transition from nodal to nodeless Zeeman splitting in altermagnets. *Phys. Rev. B* **109**, 024404 (2024).
122. Das, S., Suri, D. & Soori, A. Transport across junctions of altermagnets with normal metals and ferromagnets. *J. Phys. Condensed Matter* **35**, 435302 (2023).
123. Maier, T. A. & Okamoto, S. Weak-coupling theory of neutron scattering as a probe of altermagnetism. *Phys. Rev. B* **108**, L100402 (2023).
124. Sato, T., Haddad, S., Fulga, I. C., Assaad, F. F. & van den Brink, J. Altermagnetic anomalous Hall effect emerging from electronic correlations. *Phys. Rev. Lett.* **133**, 086503 (2024).
125. Roig, M., Kreisel, A., Yu, Y., Andersen, B. M. & Agterberg, D. F. Minimal models for altermagnetism. *Phys. Rev. B* **110**, 144412 (2024).
126. Bose, A., Vadnais, S. & Paramekanti, A. Altermagnetism and superconductivity in a multiorbital *t*–*J* model. *Phys. Rev. B* **110**, 205120 (2024).
127. Ferrari, F. & Valentí, R. Altermagnetism on the Shastry–Sutherland lattice. *Phys. Rev. B* **110**, 205140 (2024).
128. Rooj, S., Saxena, S. & Ganguli, N. Altermagnetism in the orthorhombic *Pnm* structure through group theory and DFT calculations. *Phys. Rev. B* **111**, 014434 (2025).
129. Töpfer, J. & Goodenough, J. $LaMnO_{3+\delta}$ revisited. *J. Solid State Chem.* **130**, 117–128 (1997).
130. Chen, H., Niu, Q. & Macdonald, A. H. Anomalous Hall effect arising from noncollinear antiferromagnetism. *Phys. Rev. Lett.* **112**, 017205 (2014).
This paper predicted the anomalous Hall effect in a non-collinear compensated magnet.
131. Zhou, J. et al. Predicted quantum topological Hall effect and noncoplanar antiferromagnetism in $K_{0.5}RhO_2$. *Phys. Rev. Lett.* **116**, 256601 (2016).
132. Feng, W. et al. Topological magneto-optical effects and their quantization in noncoplanar antiferromagnets. *Nat. Commun.* **11**, 118 (2020).
133. Ahn, K.-H., Hariki, A., Lee, K.-W. & Kuneš, J. Antiferromagnetism in RuO_2 as *d*-wave Pomeranchuk instability. *Phys. Rev. B* **99**, 184432 (2019).
134. Naka, M. et al. Spin current generation in organic antiferromagnets. *Nat. Commun.* **10**, 4305 (2019).
135. Guo, Y. et al. Spin-split collinear antiferromagnets: a large-scale ab-initio study. *Mater. Today Phys.* **32**, 100991 (2023).
136. Ma, H.-Y. et al. Multifunctional antiferromagnetic materials with giant piezomagnetism and noncollinear spin current. *Nat. Commun.* **12**, 2846 (2021).
137. Egorov, S. A. & Evarestov, R. A. Colossal spin splitting in the monolayer of the collinear antiferromagnet MnF_2. *J. Phys. Chem. Lett.* **12**, 2363–2369 (2021).
138. Cui, Q., Zhu, Y., Yao, X., Cui, P. & Yang, H. Giant spin-Hall and tunneling magnetoresistance effects based on a two-dimensional nonrelativistic antiferromagnetic metal. *Phys. Rev. B* **108**, 024410 (2023).
139. Chen, X., Wang, D., Li, L. & Sanyal, B. Giant spin-splitting and tunable spin-momentum locked transport in room temperature collinear antiferromagnetic semimetallic CrO monolayer. *Appl. Phys. Lett.* **123**, 022402 (2023).

140. Sødequist, J. & Olsen, T. Two-dimensional altermagnets from high throughput computational screening: symmetry requirements, chiral magnons, and spin–orbit effects. *Appl. Phys. Lett.* **124**, 182409 (2024).
141. Zhu, Y.-P. et al. Observation of plaid-like spin splitting in a noncoplanar antiferromagnet. *Nature* **626**, 523–528 (2024).
142. Zhu, Y. et al. Multipiezo effect in altermagnetic V_2SeTeO monolayer. *Nano Lett.* **24**, 472–478 (2024).
143. Wigner, E. Ueber die Operation der Zeitumkehr in der Quantenmechanik. *Nachr. Ges. Wiss. Gott. Math. Phys. Kl.* **1932**, 546–559 (1932).
144. Tang, P., Zhou, Q., Xu, G. & Zhang, S.-C. Dirac fermions in an antiferromagnetic semimetal. *Nat. Phys.* **12**, 1100–1104 (2016).
145. Šmejkal, L., Železný, J., Sinova, J. & Jungwirth, T. Electric control of Dirac quasiparticles by spin–orbit torque in an antiferromagnet. *Phys. Rev. Lett.* **118**, 106402 (2017).
146. Šmejkal, L., Mokrousov, Y., Yan, B. & MacDonald, A. H. Topological antiferromagnetic spintronics. *Nat. Phys.* **14**, 242–251 (2018).
147. Kübler, J. & Felser, C. Non-collinear antiferromagnets and the anomalous Hall effect. *Europhys. Lett.* **108**, 67001 (2014).
148. Nakatsuji, S., Kiyohara, N. & Higo, T. Large anomalous Hall effect in a non-collinear antiferromagnet at room temperature. *Nature* **527**, 212–215 (2015).
This paper reported the experimental observation of the anomalous Hall effect in a non-collinear compensated magnet.
149. Kiyohara, N., Tomita, T. & Nakatsuji, S. Giant anomalous Hall effect in the chiral antiferromagnet Mn_3Ge. *Phys. Rev. Appl.* **5**, 064009 (2016).
150. Nayak, A. K. et al. Large anomalous Hall effect driven by a nonvanishing Berry curvature in the noncolinear antiferromagnet Mn_3Ge. *Sci. Adv.* **2**, e1501870 (2016).
151. Takagi, H. et al. Spontaneous topological Hall effect induced by non-coplanar antiferromagnetic order in intercalated van der Waals materials. *Nat. Phys.* **19**, 961–968 (2023).
152. Ikhlas, M. et al. Large anomalous Nernst effect at room temperature in a chiral antiferromagnet. *Nat. Phys.* **13**, 1085–1090 (2017).
153. Li, X. et al. Anomalous Nernst and Righi-Leduc effects in Mn_3Sn: Berry curvature and entropy flow. *Phys. Rev. Lett.* **119**, 056601 (2017).
154. Higo, T. et al. Large magneto-optical Kerr effect and imaging of magnetic octupole domains in an antiferromagnetic metal. *Nat. Photon.* **12**, 73–78 (2018).
155. Matsuda, T., Kanda, N., Higo, T. & Matsunaga, R. Room-temperature terahertz anomalous Hall effect in Weyl antiferromagnet Mn_3Sn thin films. *Nat. Commun.* **11**, 909 (2020).
156. Kimata, M. et al. X-ray study of ferroic octupole order producing anomalous Hall effect. *Nat. Commun.* **12**, 5582 (2021).
157. Sakamoto, S. et al. Observation of spontaneous X-ray magnetic circular dichroism in a chiral antiferromagnet. *Phys. Rev. B* **104**, 134431 (2021).
158. Železný, J., Zhang, Y., Felser, C. & Yan, B. Spin-polarized current in noncollinear antiferromagnets. *Phys. Rev. Lett.* **119**, 187204 (2017).
159. Zhang, Y., Železný, J., Sun, Y., van den Brink, J. & Yan, B. Spin Hall effect emerging from a noncollinear magnetic lattice without spin–orbit coupling. *New J. Phys.* **20**, 073028 (2018).
160. Kimata, M. et al. Magnetic and magnetic inverse spin Hall effects in a non-collinear antiferromagnet. *Nature* **565**, 627–630 (2019).
161. Hu, S. et al. Efficient perpendicular magnetization switching by a magnetic spin Hall effect in a noncollinear antiferromagnet. *Nat. Commun.* **13**, 4447 (2022).
162. Tsai, H. et al. Electrical manipulation of a topological antiferromagnetic state. *Nature* **580**, 608–613 (2020).
163. Takeuchi, Y. et al. Chiral-spin rotation of non-collinear antiferromagnet by spin–orbit torque. *Nat. Mater.* **20**, 1364–1370 (2021).
164. Higo, T. et al. Perpendicular full switching of chiral antiferromagnetic order by current. *Nature* **607**, 474–479 (2022).
165. Pal, B. et al. Setting of the magnetic structure of chiral kagome antiferromagnets by a seeded spin–orbit torque. *Sci. Adv.* **8**, eabo5930 (2022).
166. Chen, X. et al. Octupole-driven magnetoresistance in an antiferromagnetic tunnel junction. *Nature* **613**, 490–495 (2023).
167. Qin, P. et al. Room-temperature magnetoresistance in an all-antiferromagnetic tunnel junction. *Nature* **613**, 485–489 (2023).
168. Nakatsuji, S. & Arita, R. Topological magnets: functions based on Berry phase and multipoles. *Annu. Rev. Condensed Matter Phys.* **13**, 119–142 (2022).
169. Rimmler, B. H., Pal, B. & Parkin, S. S. P. Non-collinear antiferromagnetic spintronics. *Nat. Rev. Mater.* **10**, 109–127 (2024).
170. Han, J., Yoon, J.-Y., Ohno, H. & Fukami, S. Unconventional responses in non-collinear antiferromagnets. *Newton* **1**, 100012 (2025).
171. Brekke, B., Sukhachov, P., Giil, H. G., Brataas, A. & Linder, J. Minimal models and transport properties of unconventional *p*-wave magnets. *Phys. Rev. Lett.* **133**, 236703 (2024).
172. Ezawa, M. Topological insulators and superconductors based on *p*-wave magnets: electrical control and detection of a domain wall. *Phys. Rev. B* **110**, 165429 (2024).
173. Sivianes, J., dos Santos, F. J. & Ibañez-Azpiroz, J. Optical signatures of spin symmetries in unconventional magnets. *Phys. Rev. Lett.* **134**, 196907 (2025).
174. Chakraborty, A. et al. Highly efficient non-relativistic Edelstein effect in *p*-wave magnets. *Nat. Commun.* **16**, 7270 (2023).
175. Yu, Y. et al. Odd-parity magnetism driven by antiferromagnetic exchange. *Phys. Rev. Lett.* **135**, 046701 (2025).
176. Wang, M. et al. Emergent zero-field anomalous Hall effect in a reconstructed rutile antiferromagnetic metal. *Nat. Commun.* **14**, 8240 (2023).
177. Han, L. et al. Electrical 180° switching of Néel vector in spin-splitting antiferromagnet. *Sci. Adv.* **10**, eadn0479 (2024).
178. Takagi, R. et al. Spontaneous Hall effect induced by collinear antiferromagnetic order at room temperature. *Nat. Mater.* **24**, 63–68 (2025).
179. Ray, M. K. et al. Zero-field Hall effect emerging from a non-Fermi liquid in a collinear antiferromagnet $V_{1/3}NbS_2$. *Nat. Commun.* **16**, 3532 (2025).
180. Fakhredine, A., Sattigeri, R. M., Cuono, G. & Autieri, C. Interplay between altermagnetism and nonsymmorphic symmetries generating large anomalous Hall conductivity by semi-Dirac points induced anticrossings. *Phys. Rev. B* **108**, 115138 (2023).
181. Fang, Y., Cano, J. & Ghorashi, S. A. A. Quantum geometry induced nonlinear transport in altermagnets. *Phys. Rev. Lett.* **133**, 106701 (2024).
182. Li, Y.-X., Liu, Y. & Liu, C.-C. Creation and manipulation of higher-order topological states by altermagnets. *Phys. Rev. B* **109**, L201109 (2024).
183. Zhou, X. et al. Crystal thermal transport in altermagnetic RuO_2. *Phys. Rev. Lett.s* **132**, 056701 (2024).
184. Zhan, J., Li, J., Shi, W., Chen, X. Q. & Sun, Y. Coexistence of Weyl semimetal and Weyl nodal loop semimetal phases in a collinear antiferromagnet. *Phys. Rev. B* **107**, 224402 (2023).
185. Nag, J. et al. GdAlSi: an antiferromagnetic topological Weyl semimetal with nonrelativistic spin splitting. *Phys. Rev. B* **110**, 224436 (2024).
186. Parshukov, K., Wiedmann, R. & Schnyder, A. P. Topological responses from gapped Weyl points in 2D altermagnets. *Phys. Rev. B* **111**, 224406 (2025).
187. Rao, P., Mook, A. & Knolle, J. Tunable band topology and optical conductivity in altermagnets. *Phys. Rev. B* **110**, 024425 (2024).
188. Tao, L. L. & Tsymbal, E. Y. Persistent spin texture enforced by symmetry. *Nat. Commun.* **9**, 2763 (2018).
189. Ji, J., Lou, F., Yu, R., Feng, J. S. & Xiang, H. J. Symmetry-protected full-space persistent spin texture in two-dimensional materials. *Phys. Rev. B* **105**, L041404 (2022).
190. Bernevig, B. A., Orenstein, J. & Zhang, S. C. Exact SU(2) symmetry and persistent spin helix in a spin–orbit coupled system. *Phys. Rev. Lett.* **97**, 236601 (2006).
191. Koralek, J. D. et al. Emergence of the persistent spin helix in semiconductor quantum wells. *Nature* **458**, 610–613 (2009).
192. Kuroda, K. et al. Evidence for magnetic Weyl fermions in a correlated metal. *Nat. Mater.* **16**, 1090–1095 (2017).
193. Liu, Z. Q. et al. Electrical switching of the topological anomalous Hall effect in a non-collinear antiferromagnet above room temperature. *Nat. Electron.* **1**, 172–177 (2018).
194. Xu, L. et al. Finite-temperature violation of the anomalous transverse Wiedemann–Franz law. *Sci. Adv.* **6**, eaaz3522 (2020).
195. Chen, T. et al. Anomalous transport due to Weyl fermions in the chiral antiferromagnets Mn_3X, X = Sn, Ge. *Nat. Commun.* **12**, 572 (2021).
196. Ghosh, S. et al. Raman spectroscopic evidence for linearly dispersed nodes and magnetic ordering in the topological semimetal $V_{1/3}NbS_2$. Preprint at http://arxiv.org/abs/2504.04590 (2025).
197. Sun, K., Yao, H., Fradkin, E. & Kivelson, S. A. Topological insulators and nematic phases from spontaneous symmetry breaking in 2D Fermi systems with a quadratic band crossing. *Phys. Rev. Lett.* **103**, 046811 (2009).
198. Steward, C. R. W., Fernandes, R. M. & Schmalian, J. Dynamic paramagnon-polarons in altermagnets. *Phys. Rev. B* **108**, 144418 (2023).
199. Martin, I. & Batista, C. D. Itinerant electron-driven chiral magnetic ordering and spontaneous quantum Hall effect in triangular lattice models. *Phys. Rev. Lett.* **101**, 156402 (2008).
200. *MAGNDATA: A Collection of Magnetic Structures with Portable cif-type Files*. https://www.cryst.ehu.es/magndata/.

Acknowledgements We acknowledge R. Jaeschke-Ubiergo and A. Birk Hellenes for discussions and sharing unpublished results. T.J. acknowledges support by the Ministry of Education of the Czech Republic CZ.02.01.01/00/22008/0004594 and ERC Advanced Grant number 101095925. R.M.F. acknowledges support by the Air Force Office of Scientific Research under award number FA9550-21-1-0423. J.S. and L.Š. acknowledge support by Deutsche Forschungsgemeinschaft (DFG, German Research Foundation) - DFG (Project 452301518) and TRR 288 - 422213477 (project A09). L.Š. acknowledges support by the ERC Starting Grant number 101165122. S.N. acknowledges support by the JST-MIRAI Program (JPMJMI20A1), the JST-ASPIRE Program (JPMJAP2317) and by the fund made by Canadian Institute for Advanced Research; the work at the Institute for Quantum Matter was funded by DOE, Office of Science, Basic Energy Sciences under Award number DE-SC0024469. S.M. acknowledges support by Japan Society for the Promotion of Science (JSPS), KAKENHI Grant No. JP22H00108 and No. JP24H02231.

Author contributions T.J. and L.S. wrote the initial paper. T.J., J.S., R.M.F., Q.L., H.W., S.M., S.N. and L.Š. contributed to the selection of the content, and read and commented on the paper.

Competing interests The authors declare no competing interests.

Additional information

Supplementary information The online version contains supplementary material available at https://doi.org/10.1038/s41586-025-09883-2.

Correspondence and requests for materials should be addressed to Tomas Jungwirth or Libor Šmejkal.

Peer review information *Nature* thanks Cheng Song and the other, anonymous, reviewer(s) for their contribution to the peer review of this work.